Tetrahedron: *Asymmetry* 20 (2009) 2331–2343

Contents lists available at ScienceDirect

Tetrahedron: *Asymmetry*

journal homepage: www.elsevier.com/locate/tetasy

Studies on the configuration of nitrogenous stereogenic centres in adducts of rhodium(II) tetraacylates with chiral amines: the application of ^{1}H and ^{13}C NMR spectroscopy

Jarosław Jaźwiński *, Agnieszka Sadlej

Institute of Organic Chemistry, Polish Academy of Sciences, 01-224 Warszawa, ul. Kasprzaka 44/52, Poland

ARTICLE INFO

Article history:
Received 28 July 2009
Accepted 10 September 2009
Available online 29 October 2009

ABSTRACT

The ^{1}H and ^{13}C NMR spectra of enantiomerically pure amines (*S*)-*N*,*N*-dimethyl-1-phenylethylamine, (*S*)-*N*-methyl-1-phenylethylamine, (*S*)-*N*-ethyl-1-phenylethylamine and (*S*)-*N*-ethyl-*N*-methyl-1-phenylethylamine in the presence of a twofold molar excess of dirhodium(II) tetratrifluoroacetate and dirhodium(II) Mosher's acid derivatives [(4*S*) and (4*R*)] were measured in $CDCl_3$ as a solvent. The amines having various substituents at the nitrogen atom (H, CH_3 and CH_2CH_3) formed in such conditions as an equilibrium mixture of C_SN_R and C_SN_S 1:1 adducts. The signals of both diastereoisomers were observed in NMR spectra at either room temperature (303 K) or moderately decreased temperatures (263–273 K). The rates of mutual diastereoisomer conversion were estimated by selective inversion recovery experiments and varied from less than 0.1 to ca. 10 s^{-1}, depending on the ligand and temperature. Analysis of ^{13}C NMR data and NOE experimental data resulted in the unambiguous determination of the configuration at the nitrogen atom with respect to the carbon stereogenic centre.
Modelling of adduct structures and calculations of molecular energy and NMR parameters (GIAO) using Density Functional Theory (DFT) were performed in order to support the experimental findings. The calculations were carried out using 3-21G//B3LYP (structure optimizing) and 311G(2d,p)/LanL2DZ//B3LYP theory levels (molecular energy and NMR shielding).

1. Introduction

Rhodium(II) dimeric salts (Fig. 1) are known to form adducts with a large number of organic compounds.[1] Two complexation modes of a ligand, at the axial and/or equatorial positions of the metal–metal unit, and various adduct stoichiometries yield, potentially, a large family of species.

Due to complexation properties, rhodium(II) dimeric salts have been applied in the fields of chemistry, biology and medicine. Rhodium(II) tetraacetate acting as the carbene-stabilizing agent has been used as a catalyst in organic synthesis.[2] Enantiomerically pure chiral rhodium(II) carboxylates and carboxamidates are widely used as chiral catalysts.[3,4] Some rhodium(II) salts have been able to inhibit DNA replication by binding to nucleobases; this feature has allowed the testing of these salts in medicine, as anticancer agents.[5–10] So-called dirhodium methods concern the application of rhodium(II) tetraacylates in the spectroscopy of organic compounds Due to absorption in the visible range, rhodium(II) tetraacetate and tetratrifluoroacetate have been used as the auxiliary reagents in CD spectroscopy, as sources of chromophoric groups.[11–18] Enantiomerically pure Mosher's acid salt has been used in NMR spectroscopy as chiral recognition agent allowing to determine the enantiomeric purity of chiral compounds.[19]

Dirhodium methods are based on adduct formation in situ, directly in a solution. The methods work correctly if a well-defined, stable adduct was formed. The solution instability caused by the slow adduct rearrangement and formation of an equilibrium mixture of a few species were the frequently occurring complications of dirhodium methods.[11,12] The spectra of such mixtures are usually time- and temperature-dependent. In these cases, the knowledge of the mixture composition is very helpful in the comprehension of spectral results.

Our previous investigations have included ^{1}H, ^{13}C and ^{15}N NMR studies on adducts of rhodium(II) tetraacylates with some amines in the $CDCl_3$ solution and in the solid state.[11,12,20–22] The formation of a relatively stable (in the NMR time scale) nitrogenous stereogenic centre in complexes due to the slow down of the amine inversion turned out to be the most interesting result of the work. Thus, a chiral, enantiomerically pure dirhodium salt, for example, (4*S*)-Rh_2MTPA_4 formed a mixture of two 1:1 diastereoisomers with the amine NR1R2R3 in $CDCl_3$ solution, whereas racemic *N*-methyl-1-phenylethylamine produced four 1:1 adducts. The number of isomers in the case of 1:2 adducts ($Rh_2MTPA_4L_2$) ranged from three to ten, depending on the amine. The signals of all species could be observed in NMR experiments.[21] According to Boltzmann's law, the

* Corresponding author. Tel.: +48 22 3432009; fax: +48 22 6326681.
E-mail address: jarjazw@icho.edu.pl (J. Jaźwiński).

0957-4166/$ - see front matter © 2009 Elsevier Ltd. All rights reserved.
doi:10.1016/j.tetasy.2009.09.021

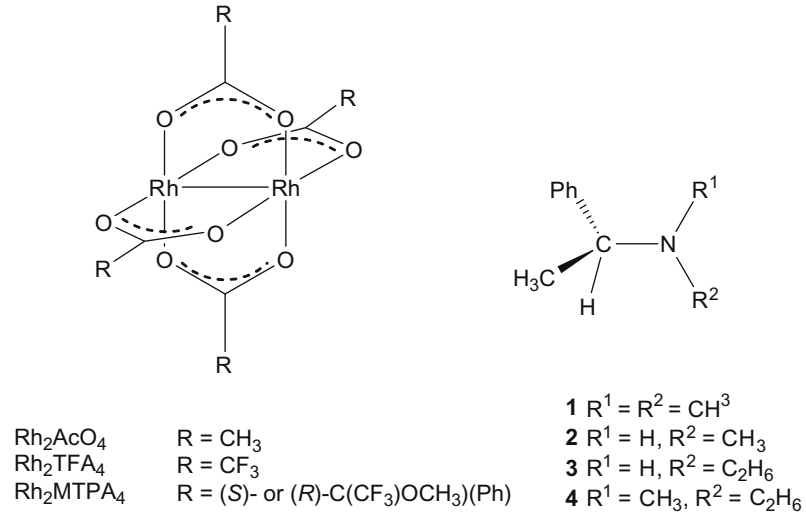

Rh_2AcO_4 R = CH_3
Rh_2TFA_4 R = CF_3
Rh_2MTPA_4 R = (*S*)- or (*R*)-C(CF_3)OCH_3)(Ph)

1 $R^1 = R^2 = CH^3$
2 R^1 = H, $R^2 = CH_3$
3 R^1 = H, $R^2 = C_2H_6$
4 $R^1 = CH_3$, $R^2 = C_2H_6$

Figure 1. Dimeric rhodium(II) tetraacylates and amines used as ligands (MTPA-H ≡ α-methoxy-α-(trifluoromethyl)-phenylacetic acid = Mosher's acid).

constitution of such an equilibrium mixture was expected to be temperature-dependent.

Adducts of some chiral amines R*-NR1R2 (R* denotes a group having a carbon stereogenic centre) with rhodium(II) tetraacylates were the subject of the present investigations. This included the application of ^{1}H NMR and ^{13}C NMR techniques to establish the configuration at the nitrogen atom in relation to the carbon stereogenic centre. Enantiomerically pure amines (*S*)-*N*,*N*-dimethyl-1-phenylethylamine **1**, (*S*)-*N*-methyl-1-phenylethylamine **2**, (*S*)-*N*-ethyl-1-phenylethylamine **3** and (*S*)-*N*-ethyl-*N*-methyl-1-phenylethylamine **4** were selected as ligands; three rhodium(II) salts, Rh_2TFA_4, (4*S*)- and (4*R*)-Rh_2MTPA_4 were used as substrates.

2. Results and discussion

2.1. Adducts of (*S*)-*N*,*N*-dimethyl-1-phenylethylamine 1

(*S*)-*N*,*N*-Dimethyl-1-phenylethylamine **1** was the first ligand under consideration used in the present work as a model in order to test our research methods. Some NMR data concerning adducts of **1** have been reported previously.[20] Rhodium(II) tetratrifluoroacetate formed with **1** the 1:1 or/and 1:2 adducts, depending on the components' molar ratio in solution. ^{1}H NMR spectra showed up four groups of signals (Table 1); from them $N(CH_3)_2$ peaks were the most interesting. *N*-Methyl groups produced two signals in the ^{1}H NMR spectrum, since these groups were chemically non-equivalent in the adduct. The appearance of $N(CH_3)_2$ signals depended on the molar ratio of Rh_2TFA_4 to **1** in the solution and the sample temperature (Fig. 2). The 1:0.5 mixture assured the presence of a 1:1 adduct in the solution (and an excess of Rh_2TFA_4). Consequently two *N*-methyl signals appeared in the ^{1}H NMR spectrum. This was the only sample that exhibited narrow signals over the whole temperature range, from 268 to 318 K. The 1:1.33 mixture showed up to four NCH_3 signals (268 K), approximately of the same intensity, derived from the 1:1 and 1:2 adducts. The 1:2 mixture contained solely the 1:2 adduct and provided two NCH_3 signals. Finally, the 1:4 mixture showed two NCH_3 signals originating from the 1:2 adduct and one peak produced by non-complexed amine.

A few exchange processes were potentially possible in the solutions: the exchange of **1** between the 1:1 adduct and dirhodium salt in the 1:0.5 solution; the exchange involving 1:1 and 1:2 adducts; and the exchange between the 1:2 adduct and free amine in the presence of an excess of ligand. Simultaneously, the mutual exchange of two non-equivalent $N(CH_3)_2$ groups was expected. Such exchanges (pro-*R* to pro-*S* and vice versa) occurred either by the attack of the rhodium salt to the nitrogen atom in the adduct and structure inversion (S_N2-like mechanism) or via adduct dissociation, ligand inversion and adduct recombination.[19] The rate of pro-*R*/pro-*S* exchange of NCH_3 indicated the stability of the particular configuration at the nitrogen atom. The question arose as to whether the lifetime of a structure was sufficiently long enough to identify the *N*-methyl groups (i.e., which one is pro-*R*, and which one is pro-*S*), or establish the configuration of the nitrogenous stereogenic centre by NMR methods. The answer was not obvious; it should be noted that **1** in an Rh_2AcO_4 solution, regardless of temperature and stoichiometry, shows one singlet originating from both $N(CH_3)_2$ groups.[20]

Herein, exchange processes were examined by a method based on the selective inversion of one signal and observation of signals evolution with time.[23,24] The inspection of a non-perturbed signal was the most convenient means for the detection of an exchange. Theoretically, if no exchange takes place, the intensity of this signal should be independent of time. In practice, some signal enhancement was possible due to NOE between two groups attached to the same atom. The evolution of *N*-methyl signals in Rh_2TFA_4 and **1** solution at various temperatures was shown in Figure 3. For the 1:1 adduct (Fig. 3a and b), the curves corresponding to the non-inverted signal revealed the decrease of the pro-*R*/pro-*S* exchange rate with temperature reduction, up to very low value at 273 K. In case of the 1:1.33 mixture, containing two adducts, the inversion of one signal in the 1:2 adduct (Fig. 3c) caused two different responses of two *N*-methyl signals in the 1:1 adduct. This asymmetry became obvious if one considered the fact that the polarization of *N*-methyl groups was retained when the 1:2 adduct lost the ligand producing a 1:1 adduct. The curve, corresponding to the pro-*R*/pro-*S* mutual exchange in the 1:2 adduct, can be seen between these two lines arising from ligand exchanges. Finally, for the 1:4 mixture, containing the 1:2 adduct and non-bonded (free) ligand **1** (Fig. 3d), the inversion of the NCH_3 signal in **1** resulted in the equal response of both NCH_3 signals in the adduct.

For an equally populated, two-site exchange system, an exchange rate *k* may be calculated by curve fitting, by the application of either Eq. (2) to the inverted signal or Eq. (3) to non-perturbed signal. Depending on the experiment and signals used for the

Table 1
^{1}H and ^{13}C NMR chemical shifts for adducts of some amines with dirhodium salts[a]

Adduct		T (K)	CH	CCH_3	NH	NCH_3	NCH_2CH_3	NCH_2CH_3
Rh_2TFA_4-**1**		303	4.80(67.0)	1.69(17.9)	—	2.84(38.8)[b] 2.62(48.5)[c]		
		268	4.79	1.66	—	2.82, 2.59		
		268[d]	4.86[d]	1.68[d]	—	2.88[d], 2.70[d]		
Rh_2TFA_4-**2**	N_R	263	4.97(59.5)	1.80(14.2)	5.41	2.86(30.7)		
	N_S		4.60(63.8)	1.66(22.3)	5.19	2.67(38.0)		
(4*S*)-Rh_2MTPA_4-**2**	N_R	303	5.16(58.8)	1.84(13.2)	5.29	2.90(29.8)		
	N_S		4.67(63.7)	1.74(23.2)	5.02	2.68(37.8)		
(4*S*)-Rh_2MTPA_4-**3**	N_R	273	5.05(58.1)	1.84(13.9)	4.90	—	3.47, 3.25(39.8)	1.07(15.1)
	N_S		4.71(61.5)	1.67(23.2)	4.86	—	3.19, 3.02(44.8)[e]	1.15(14.2)
(4*R*)-Rh_2MTPA_4-**3**	N_R	273	5.01(58.4)	1.97(14.0)	4.88	—	3.45, 3.24(39.9)	1.08(15.1)
	N_S		4.65(61.6)	1.70(23.0)	4.85	—	3.30, 3.15(44.7)[e]	1.12(14.4)
Rh_2TFA_4-**4**	N_R	273	4.71[e](69.3)	1.72(18.6)	—	2.59(43.8)	3.78, 3.00(47.7)	1.13(9.9)
	N_S		4.75(68.3)	1.60(18.4)	—	2.87(35.5)	3.36, 2.69(55.6)	0.95(10.4)
(4*S*)-Rh_2MTPA_4-**4**	N_R	303	4.92(69.1)	1.73(19.4)	—	2.65(44.0)	3.81[e], 3.28[e](48.0)	1.21(10.6)
	N_S		4.92(68.5)	1.73(19.4)	—	3.00[e](35.3)	3.48, 2.83(55.6)	0.89(10.9)
(4*R*)-Rh_2MTPA_4-**4**	N_R	303	4.86[e](69.2)	1.74(19.2)	—	2.71(43.8)	3.78, 3.10[e](48.0)	1.17(10.3)
	N_S		4.88[e](68.2)	1.70(19.4)	—	3.02(35.4)	3.50, 3.00[e](55.2)	0.86(10.5)

[a] All measurements were performed in $CDCl_3$ solutions containing dirhodium salt and ligand in a molar ratio of 1:0.5 (if not marked otherwise); ^{1}H (^{13}C) chemical shifts (ppm) are given with respect to the $CHCl_3$ residual signal (^{1}H, 7.26 ppm,) or $CDCl_3$ central peak (^{13}C, 77.0 ppm). Chemical shifts of the main adduct in each mixture are underlined. Chemical shifts of Ph groups, if assigned and identified, are as follows (Ph *ipso*, *ortho*, *meta* and *para* protons are denoted as C^i *o*, *m* and *p*, respectively): Rh_2TFA_4-**1**; 303 K: (147.1)C^i, 7.60(130.2)*o*, 7.51(128.3)*m*, 7.48(126.3)*p*; 268 K: 7.61*o*; 268 K. Adduct 1:2: 7.52*o*; Rh_2TFA_4-**2**, C_SN_R: 7.61(126.9)*o*, 7.53(128.3)*m*, 7.44(127.9)*p*; C_SN_S adduct shows practically the same chemical shifts; (4*S*)-Rh_2MTPA_4-**2**, C_SN_R: 7.58*o*, 3.11 OCH_3; C_SN_S: 7.53*o*, 3.12 OCH_3; (4*S*)-Rh_2MTPA_4-**3**, C_SN_R: 7.57(127.4)*o*, 7.46(129.2)*p*, 7.40(127.9)*m*, 3.08 OCH_3; C_SN_S: 3.10 OCH_3; (4*R*)-Rh_2MTPA_4-**3**, C_SN_R: 7.52(127.4)*o*, 7.44(129.1)*m*, 7.40(128.0)*p*, 3.08 OCH_3; C_SN_S: 3.10 OCH_3; Rh_2TFA_4-**4,** (4*S*)-Rh_2MTPA_4-**4** and (4*S*)-Rh_2MTPA_4-**4**: not assigned. The reference data of free ligands are as follow: **1**:[7a] 1.38(20.1) CCH_3; 2.20(43.1) NCH_3; 3.25(65.9) CH; 7.30 (127.4, 128.1)*o*,*m*, 7.23(126.8)*p*, (144.0)C^i **2**:[7a] 1.33(23.8) CCH_3; 2.31(34.5) NCH_3; 3.64(60.2) CH; 7.31(128.4, 126.5)*o*,*m*; 7.24(126.8)*p*; (145.4)C^i; NH not observed. **3**: 1.11(15.2) CH_2CH_3; 1.39(24.1) CCH_3; 2.52, 2.57(41.8) CH_2CH_3; 3.81(58.1) CH; 7.06–7.24(126.3, 126.6, 128.2)*o*,*m*,*p*; 145.7C^i; **4**: 1.09(12.0)*v*CH_2CH_3; 1.42(19.0) CCH_3; 2.25(37.9) NCH_3; 2.40, 2.56(48.1) CH_2CH_3; 3.60(63.1) CH; 7.25–7.41(126.6, 127.5, 128.0)*o*,*m*,*p*; 144.1C^i.

[b] Pro-*R* methyl group.

[c] Pro-*S* methyl group.

[d] 1:2 Adduct.

[e] Signals were identified by means of 2D ^{1}H, ^{1}H COSY or ^{13}C, ^{1}H gHSQC spectra.

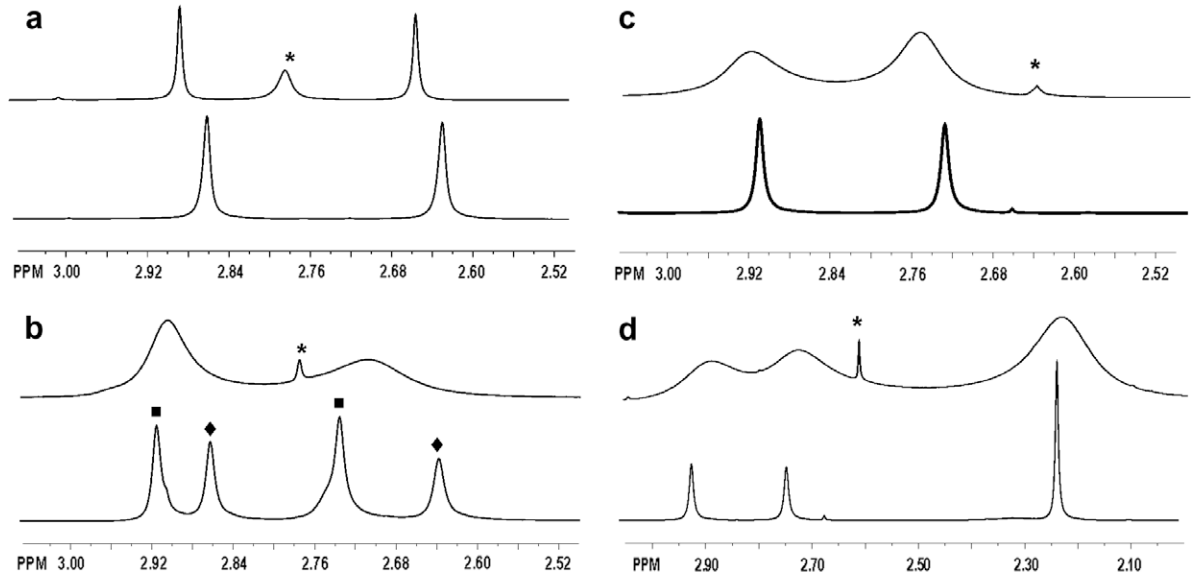

Figure 2. The ^{1}H NMR signals of *N*-methyl groups in various Rh_2TFA_4 and **1** mixtures ($CDCl_3$ solutions), at 303 K (upper traces) and 268 K (lower traces). The spectra represent the Rh_2TFA_4 and **1** solution in molar ratio of 1:0.5 (a), 1:1.33 (b), 1:2 (c) and 1:4 (d). Diamonds ♦ and squares ■ indicate the signals of the 1:1 and 1:2 adducts, respectively; and asterisks (*) indicate the signals of impurity or water. Vertical scales were adjusted arbitrarily.

calculations, one can obtain two quantities: the rate of the mutual exchange of the two *N*-methyl groups (pro-*R*/pro-*S* exchange) or the rates of ligand exchange between species. Thus, for a 1:0.5 sample (i.e., for a sample containing the 1:1 adduct only) curve fittings provided the rate of pro-*R*/pro-*S* exchange from 0.6 to 1.0 s^{-1} (318 K) and from 0.1 to 0.3 s^{-1} (303 K), depending on which signal was inverted and which data set was used for the calculations. For low temperature experiments (288 K and below) the calculations failed; nevertheless a rough estimation suggested the rate k to be much less than 0.1 s^{-1}. Similar procedures when applied to the 1:2 sample (268 K) provided the rates from 0.8 to 2.3 s^{-1} for the 1:2 adduct.

The 1:4 mixture contains equimolar quantities of bonded and free amine **1**; thus the signals of CCH_3 groups form an equally

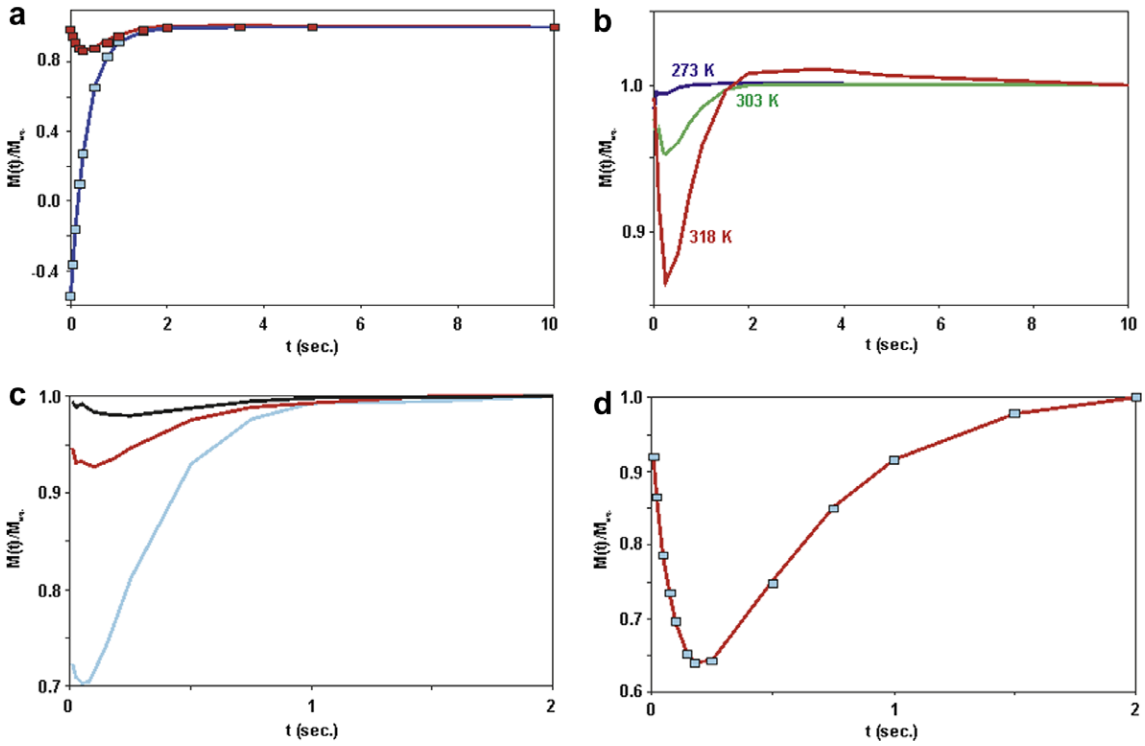

Figure 3. Selective inversion recovery experiments: evolution with time of *N*-methyl signals in Rh_2TFA_4-**1** adducts: (a) 1:0.5 mixture, 318 K; blue and red curves represent the evolution of inverted and non-perturbed signals, respectively; points represent fitted lines; (b) 1:0.5 mixture, the evolution of non-perturbed signal at 318 K (red), 303 K (green) and 273 K (blue line). Note different vertical scale in plot (a) and (b); (c) 1:1.33 mixture, 268 K; the evolution of non-perturbed signals of the 1:1 adduct (blue and black curves) and one signal of the 1:2 adduct (red) while the second signal was inverted; (d) 1:4 mixture, 268 K; the evolution of two signals of the 1:2 adduct (red line and blue points) while the signal of non-bonded amine was inverted; the signals perfectly overlapped.

two-site populated system, meaning Eqs. (2) and (3) could be applied. The exchange rate of **1** between an adduct and a solution was found to be from 2.2 to 3.2 s^{-1}. Unfortunately, a similar procedure was not useful in case of 1:1.33 solution (containing the 1:1 and 1:2 adducts), due to CCH_3 signals overlapping.

2D EXSY technique was expected to give an insight into the overall exchange pattern. The EXSY spectrum of the 1:0.5 solution taken at room temperature (303 K) contained positive off-diagonal peaks corresponding to the pro-*R*/pro-*S* exchange of the *N*-methyl groups. These peaks vanished at 288 K due to an exchange slow down and became negative at 268 K because of dominance of the NOE enhancement over exchange effects. The sum of rates $k + k_{-1}$ estimated on the basis of peak integrations[24] was found to be 0.3 s^{-1} at 303 K. Similar experiments performed for the 1:2 adduct provided the $k + k_{-1}$ value of 2.1 s^{-1} at 268 K. This means that the exchange is faster than that in the 1:1 adduct ($k \ll 0.1$ s^{-1} at 273 K).

The remaining samples (1:1.33 and 1:4) showed up more complicated spectra (Fig. 4). The on-diagonal *N*-methyl signal in the 1:2 adduct (1:1.33 mixture) (Fig. 4a) correlated with the second NCH_3 peak (pro-*R*/pro-*S* exchange), and with two NCH_3 signals of the 1:1 adduct (ligand exchange). The various intensities of these signals were caused by three different exchange rates. The lack of a peak attributed to the pro-*R*/pro-*S* exchange in the 1:1 adduct was an interesting feature of this spectrum. The same effect appeared in the spectrum of the 1:4 sample (Fig. 4b); a peak corresponding to the pro-*R*/pro-*S* exchange was weak in comparison to the other signals. Such a pattern suggested that the mechanism of this exchange was not the direct NCH_3 exchange in an adduct but an exchange via adduct—free ligand—adduct. The ligand exchange rate, calculated on the basis of CCH_3 signals, was found to be 5.1 s^{-1} ($k + k_{-1}$); similar value (5.2 s^{-1}) provided CH signals.

This led us to the following conclusions: (i) *N*-methyl groups in the adducts underwent mutual exchange (pro-*R*/pro-*S* exchange) with rates varying from 0.1 s^{-1} to ca. 2 s^{-1}, depending on the temperature and on Rh_2TFA_4 to ligand molar ratio; (ii) pro-*R*/pro-*S* exchange in the 1:1 adduct was very slow at the reduced temperature ($k \ll 0.1$ s^{-1} below 288 K); (iii) consequently, the lifetime $1/k$ of a particular configuration varied from 0.5 to a few seconds, and was long in comparison to the ^1H spin-lattice relaxation time T_1 (Table 2). It is important to note the following: the aforementioned pro-*R*/pro-*S* exchange rate probably did not describe a single process, but it was the outcome of several factors. The slow pro-*R*/pro-*S* exchange did not imply the long lifetime of the particular conformer. Finally, the ligand exchange rate and pro-*R*/pro-*S* exchange rate concerned two different processes. This differentiation is important in the next parts of the work. The measurements of the exchange rates in C_SN_R/C_SN_S adduct mixture (e.g., adducts of **2**, **3** and **4**, see below) provided the diastereomerization rate, which is generally different to the ligand exchange rate.

In the next stage of work, DFT calculations were performed. The structures of three Rh_2TFA_4-**1** conformers (Fig. 5) were optimized and the corresponding energies and NMR parameters were calculated. The energies were calculated assuming either a single molecule in vacuum or solvation ($CHCl_3$, IEFPCM model). Both approaches unambiguously indicated that the conformer **I** is privileged (>99% at 303 K). ^1H NMR NOE experiments (DPFGSE-NOE) agreed with the theoretical findings (Fig. 6). Inversion of low shift NCH_3 signal resulted in the enhancement of Ph_{ortho} and CH signals; and inversion of the second NCH_3 enhanced the Ph_{ortho} and CCH_3 signals. The remaining experiments confirmed these interactions, since instant inversion of the Ph_{ortho} signal resulted in the answer of both *N*-methyl peaks. The different behaviour of the NCH_3 signals at various temperatures was an interesting result of the exper-

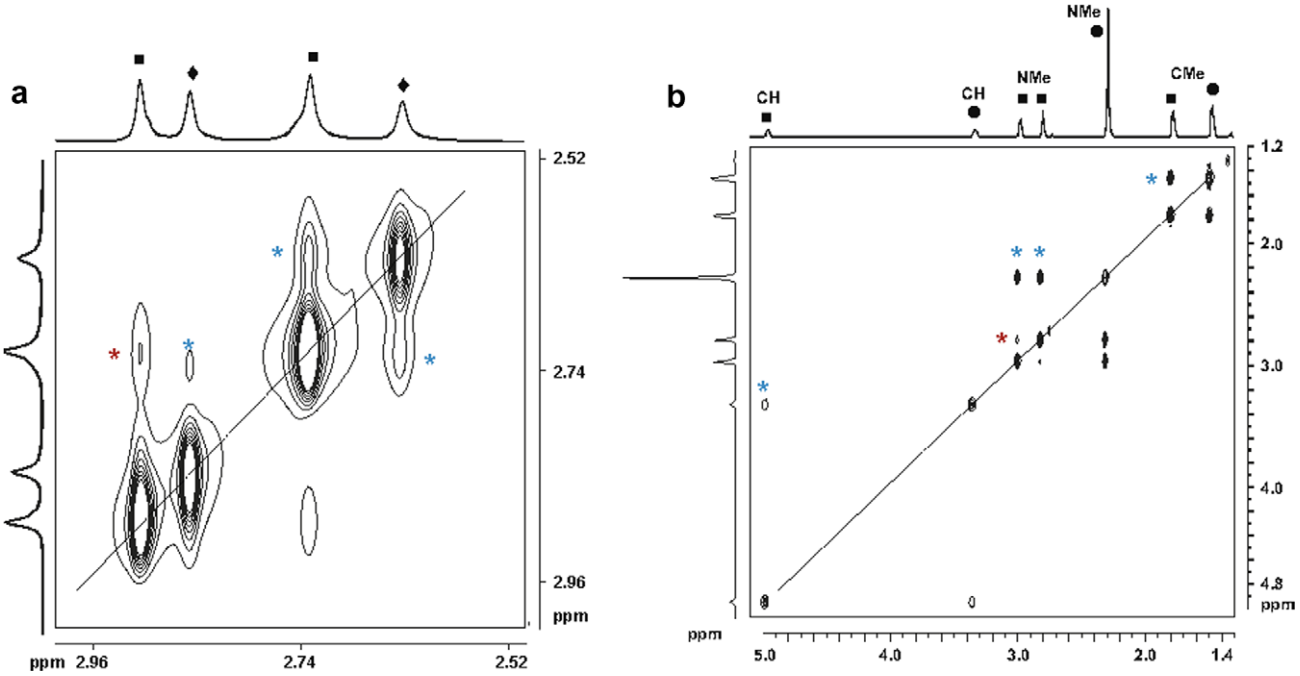

Figure 4. EXSY spectra of Rh_2TFA_4: **1** solution (268 K): (a) 1:1.33 sample (NCH_3 region); (b) 1:4 solution (aliphatic region). Diamonds (♦) indicate the signals of the 1:1 adduct; squares (■) denote the signals of the 1:2 adduct, and circles (●) indicate the signals of non-complexed ligand **1**. Off-diagonal signals corresponding to the pro-*R*/pro-*S* exchange are indicated by red asterisks; and the signals related to the ligand exchange are indicated by blue asterisks.

Table 2
Non-selective and bi-selective (in parentheses) ^1H longitudinal relaxation times T_1 (s) in Rh_2TFA_4-**1** at various temperatures[a]

T (K)	Ph_{ortho}	CH	CCH_3	NH	NCH_3
273	0.669	0.566	0.399		0.235 (0.217) 0.226 (0.213)
288	0.817	0.771	0.771		0.285 (0.299) 0.263 (0.275)
303	1.006	0.924	0.924		0.362 (0.382) 0.329 (0.340)
318	1.189	1.067	1.067		0.447 (0.466) 0.408 (0.415)

[a] All samples contained a $CDCl_3$ solution of Rh_2TFA_4 and **1** in a molar ratio of 1:0.5. The measurements were performed using either non-selective or selective inversion recovery sequence.

iment. At low temperature, while one NCH_3 signal was inverted, the second one was positive because of an NOE enhancement. However, at room temperature this signal was negative, due to the domination of exchange (i.e., saturation transfer) over the NOE.

The calculated ^1H and ^{13}C chemical shifts for three conformers are shown in Table 3. The calculations were performed both for a single molecule and assuming solvation ($CHCl_3$, IEFPCM solvation model). Generally, it is known that calculated chemical shifts differ from experimental data; the differences depend on the method and basis set used for the calculations.[25] On the other hand, theoretical and experimental data sets should satisfy the equation $\delta_{calc} = a\delta exp + b$. Herein, a correlation coefficient and standard errors were used as criteria of correctness of the structure identification. The best correlation between the observed and calculated shifts was found for conformer **I**, although the differences were rather small (Table 3). Standard errors associated with linear regression, measuring how closely data points spread about the regression line, were more diversified, and unambiguously indicated to conformer **I**. No significant differences between solvated and non-solvated molecules occurred.

Finally, we attempted to estimate the distances between the hydrogen atoms in the adduct by the use of NOE build-up measurements. It is known that this technique provides rather inaccurate results for flexible molecules.[26] On the other hand, in the case

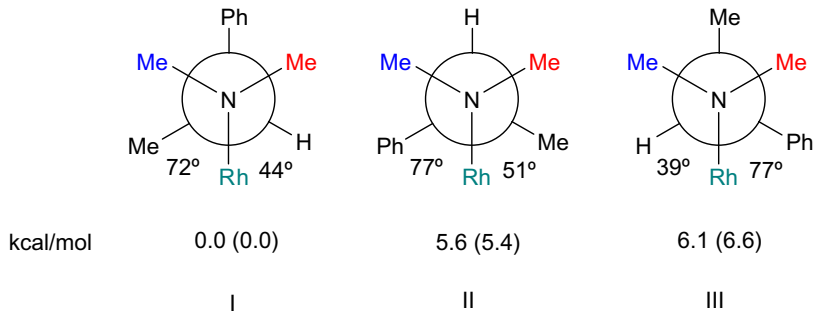

Figure 5. Three conformers of the 1:1 Rh_2TFA_4-**1** adduct were used as input for structure optimizations (for the sake of clarity, one Rh atom was shown), relative molecular energies and some structural parameters (dihedral angles Rh–N–C–CH_3, Rh–N–C–H, Rh–N–C–C^i). Energy calculations were performed for optimized structures applying either single molecule in vacuum or assuming the IEFPCM ($CHCl_3$) solvation model (in parentheses). The energy of **I** was assumed to be 0.0 kcal/mol.

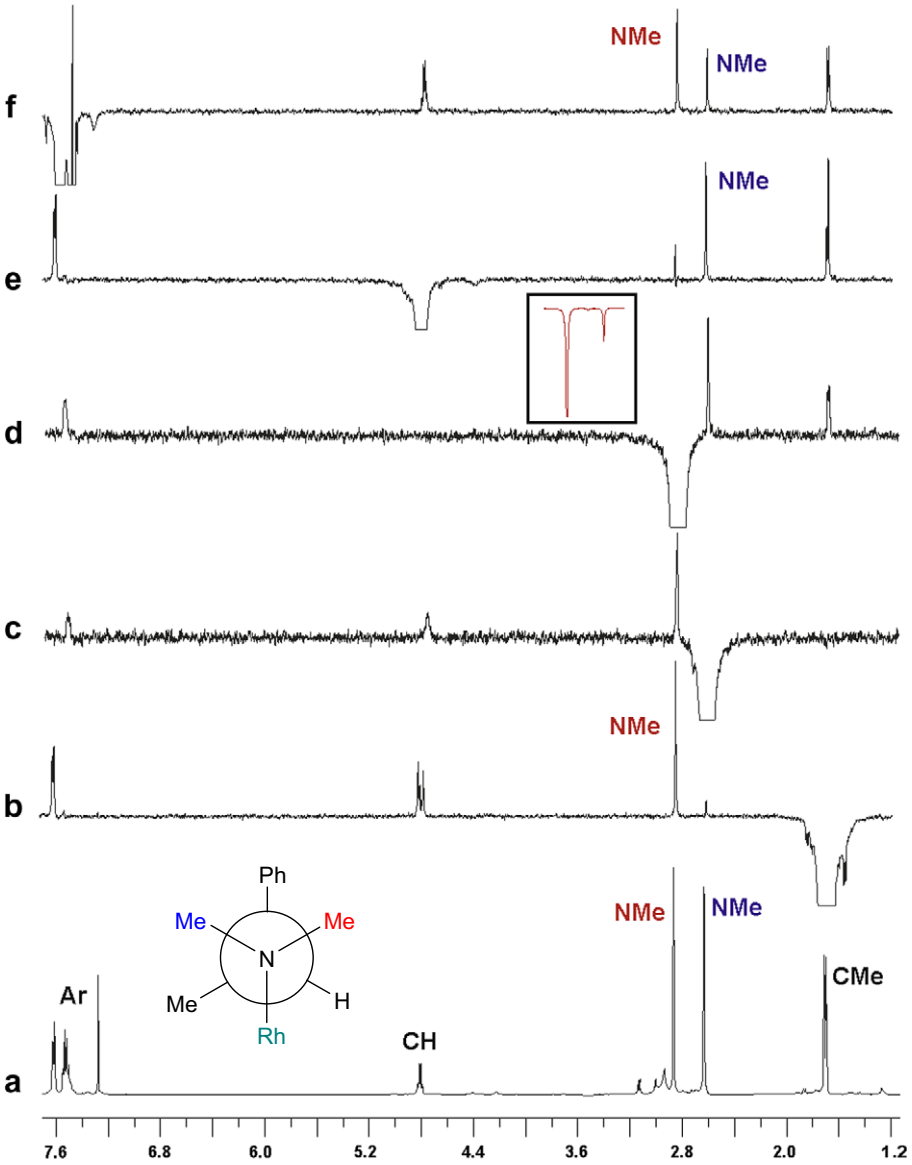

Figure 6. ^{1}H NMR (DPFGSE-NOE) spectra of the 1:1 Rh_2TFA_4-**1** adduct, at 268 K. The inset shows NCH_3 signals in the spectrum taken at 303 K, while high-frequency NCH_3 signal is inverted. Dominance of the NOE enhancement over exchange effects at low temperature is clearly visible.

of Rh_2TFA_4-**1**, the lifetime of the adduct was long, and one conformer was privileged. Averaged distances ($\langle d^{-3}\rangle^{-1/3}$)[26] between CH, Ph_{ortho} and CH_3 groups for optimized structures **I**–**III**, NOE build-up rates and some estimated H–H distances were collected in Table 4 (see Section 4 for the details). The measurements provided reasonable, but rather qualitative results. For example, expected Ph_{ortho}–NCH_3 (pro-*S*) and Ph_{ortho}–NCH_3 (pro-*R*) distances were 3.61 and 3.41 Å, while the values of 3.64 and 3.35 Å were obtained from an NOE build-up using Ph_{ortho}–CCH_3 distance as a reference.

The NULL technique is another approach to H–H distance determination.[27] The method is based on the measurements of two relaxation times: total T_1, by conventional inversion recovery technique, and selective T_{1sel}, with inversion of all signals, except one. The differences $1/T_{1sel} - 1/T_1$ are proportional to H–H distances to an atom in question. However, this method failed in the case of Rh_2TFA_4-**1** adduct, probably due to the short ^{1}H relaxation time T_1. The experiment was repeated twice and the linear correlation between two sets of $(1/T_{1sel} - 1/T_1)$ values was expected. In fact the correlation was very poor (correlation coefficient of 0.6) indicating that the experimental error was comparable with the measured values.

2.2. Adducts of (*S*)-*N*-methyl-1-phenylethylamine 2

Some ^{1}H, ^{13}C and ^{15}N NMR chemical shifts of Rh_2TFA_4 and Rh_2MTPA_4 adducts with **2** were reported previously.[20,21] The measurements taken at reduced temperature revealed that **2** forms two 1:1 adducts with each of the above dirhodium salts. However, the configuration of the nitrogenous stereogenic centre in these adducts was not determined.

The Rh_2TFA_4-**2** adduct appeared to be unstable and decomposes in the $CDCl_3$ solution within 1–2 h, despite the low temperature of measurement (263 K). The application of advanced, time consuming NMR techniques was difficult in this case. Nevertheless, the determination of configuration at the nitrogen atom on the basis of experimental ^{1}H and ^{13}C chemical shifts and some results of theoretical computations was attempted. At first, six possible structures of Rh_2TFA_4-**2** were optimized and their molecular energies were computed (Fig. 7). The calculations unambiguously pointed

Table 3
Calculated ^{1}H and ^{13}C NMR chemical shifts for three hypothetical conformers of 1:1 Rh_2TFA_4-**1** and two diastereoisomers of Rh_2TFA_4-**2**[a]

	Ph(C^i)	Ph_{ortho}	Ph_{meta}	Ph_{para}	CH	CCH_3	NCH_3[b]	R[c]	rms[c]
I	(146.1)	7.78(134.5)	7.72(133.7)	7.70(134.1)	5.12(75.9)	1.62(20.7)	3.14(41.1) 2.71(50.9)	0.999(0.998)	0.13(3.6)
I ($CHCl_3$)	(145.9)	7.93(134.7)	7.92(134.0)	7.90(134.5)	5.13(76.1)	1.62(20.4)	3.17(41.2) 2.72(50.8)	0.999(0.998)	0.12(3.7)
II	(146.1)	7.98(135.4)	7.52(133.3)	7.55(133.7)	4.18(85.8)	1.97(19.0)	2.62(51.9) 3.27(52.4)	0.991(0.992)	0.38(6.8)
II ($CHCl_3$)	(146.9)	8.09(135.7)	7.64(133.2)	7.71(133.6)	4.51(84.6)	1.95(19.1)	2.64(51.6) 3.31(52.0)	0.995(0.993)	0.30(6.2)
III	(145.0)	7.79(135.3)	7.48(133.7)	7.52(133.7)	5.60(71.1)	1.80(18.1)	3.31(51.3) 2.90(44.4)	0.994(0.994)	0.30(5.8)
III ($CHCl_3$)	(145.7)	7.87(135.5)	7.62(133.6)	7.68(133.6)	5.58(71.4)	1.87(17.9)	3.35(51.3) 2.94(44.1)	0.996(0.994)	0.25(5.8)
IV ($CHCl_3$)	(147.2)	7.93(132.8)	7.98(134.7)	7.93(134.4)	5.32(66.8)	1.63(13.6)	3.11(30.7)	0.999(0.999)[d,e]	0.15(2.4)[d,e]
VII ($CHCl_3$)	(149.1)	7.89(132.8)	7.90(134.3)	7.86(134.1)	4.87(71.0)	1.56(24.7)	2.83(39.3)	1.000(0.999)[f,e]	0.10(1.8)[f,e]

[a] ^{1}H and ^{13}C chemical shifts are given in ppm. Calculations were performed for both single molecule in the vacuum and molecule in $CHCl_3$ (IEF PCM solvation model). All data concerning ^{13}C are given in parentheses.
[b] Signals arising from pro-*R* *N*-methyl group were underlined.
[c] Correlation coefficients *R* and rms were obtained from the least-square linear regression performed for each set of calculated and experimental (303 K, $CDCl_3$, Rh_2TFA_4 and **1** with molar ratio of 1: 0.5, Table 1) data.
[d] The correlation between calculated data for **IV** and experimental data for the isomer identified as C_SN_R (Table 1). Reverse correlation (**IV** and C_SN_S provided *R* of 0.999(0.997) and rms of 0.25(2.7).
[e] The correlation between all calculated (**IV** and **VII**) and experimental (C_SN_R and C_SN_S) data assuming the assignments like those in Table 1 provided *R* and rms of 0.999(0.999) and 0.12(2.0); opposite assignment resulted in the values of 0.996(0.993) and 0.25(6.3).
[f] The correlation between calculated data for **VII** and experimental data for the isomer identified as C_SN_S (Table 1). Reverse correlation (**VII** and C_SN_R provided *R* of 0.999(1.000) and rms of 0.12(1.5).

Table 4
Averaged distances (Å) between CH, Ph_{ortho} and CH_3 groups for three hypothetical conformers **I–III** and NOE build-up rates

Averaged distance[a]	I	II	III	NOE build-up rate[b]	Calculated distances (Å)[c]
CH–NCH_3	3.00	2.96	3.85	8.1 NCH_3(CH); 6.4 CH(NCH_3)	2.65
CH–*NCH_3*	3.86	2.72	3.09	0.8 *NCH_3*(CH); n.o. CH(NCH_3)	3.74
CH–CCH_3	2.61	2.63	2.64	6.9 CCH_3(CH); 8.9 CH(CCH_3)	2.61
H–Ph	2.69	2.67	2.77	7.1 Ph(CH); 9.3 CH(Ph)	
Ph–NCH_3	3.61	4.87	3.32	4.8 NCH_3(Ph); 4.6 Ph (NCH_3)	3.63
Ph–*NCH_3*	3.41	3.62	4.9	7.3 *NCH_3*(Ph); 8.2 Ph (NCH_3)	3.34
Ph–CCH_3	3.26	3.33	3.19	9.4 CCH_3(Ph); 8.6 Ph (CCH_3)	3.26
CCH_3–NCH_3	4.76	3.26	3.05	0.8 NCH_3(CCH_3); n.o.CCH_3(NCH_3)	4.95
CCH_3–*NCH_3*	3.17	4.74	3.68	10.7 *NCH_3*(CCH_3); 11.5CCH_3(*NCH_3*)	3.21
NCH_3–NCH_3	3.08	3.06	3.08	13.8 NCH_3(*NCH_3*); 14.5 *NCH_3*(NCH_3)	3.08

[a] Averaged distances (Å) between hydrogens in CH, Ph and CH_3 groups calculated on the basis of optimized structures according to the formula $(\langle d^{-3}\rangle^{-1/3})$[11]; see Section 4 for the details. Only *ortho*-hydrogens of Ph group were considered. Pro-*R* *N*-methyl signals are given in italics. n.o. means 'not observed'.
[b] The pair of interacted groups are given in each row; the observed and inverted (in parentheses) signals were indicated next to each values.
[c] Reference distance is double-underlined.

to the diastereoisomers **IV** and **VII** as the structures with the lowest energy. However, the theoretical calculations did not decide which isomer (**IV** or **VII**) was preferred, since their minimal molecular energy depended on which model (isolated or solvated molecule) was applied. In the next step the calculations of ^{1}H and ^{13}C chemical shifts for **IV** and **VII** were performed (Table 3). The correlations between the theoretical and experimental data sets for a single compound did not solve the problem, since all combinations of data (i.e., C_SN_R Rh_2TFA_4-**2** vs **IV**, or C_SN_R vs **VII**, etc.) did not provide decisive differences with regard to the coefficients *R* and rms. Overall regression using the data of both diastereoisomers at once (**IV** and **VII** vs C_SN_R and C_SN_S) appeared to be more diagnostic (Table 3). The analysis of C^{13} chemical shifts provided subsequent evidence: the chemical shift differences between major and minor components of Rh_2TFA_4-**2** (−4.3, −8.1 and −7.3 ppm for CH, CCH_3 and NCH_3, respectively) followed the corresponding differences between **IV** and **VII** (−4.2, −11.1 and −8.6 ppm). Hence, these findings showed that isomer **IV** (C_SN_R) as the major component and **VII** (C_SN_S) as the minor component of the Rh_2TFA_4-**2** mixture.

The ^{1}H NMR spectrum of the (4*S*)-Rh_2MTPA_4 and **2** 1:0.5 mixture showed the signals of two adducts, in the molar ratio of 1–5.3 (Fig. 8). Although the optimizations of (4*S*)-Rh_2MTPA_4-**2** structures were not performed due to large molecule and computing limitations, it was tentatively assumed that the previous findings (i.e., for Rh_2TFA_4-**2**) were valid in this case too. Hence, (4*S*)-Rh_2MTPA_4-**2** adducts were expected to adopt the structures **IV** and **VII**. Diastereomerization rates of 0.2 and 0.8 s^{-1} (at 303 K) for forward and reverse processes were estimated on the basis of selective inversion recovery experiments; hence diastereoisomer lifetimes came to seconds.

Vicinal ^{3}J(CH–NH) coupling constants provided a preliminary argument indicating the configuration at the nitrogen atom.[21] The CH and NH signals of the major adduct appeared as quartets, split by coupling with CH_3 groups. Vicinal NH–CH coupling, of ca. 1.5 Hz, appeared as line broadening only: half-widths of the line in NCH_3 and NCH_3 doublets came to 2.5 Hz, whereas for CH and NH quartets this value reached 4 Hz. In contrast, the NH and CH signals of the minor adduct were more complicated due to the large vicinal coupling, of ca. 10 Hz (Fig. 8). According to Karplus'

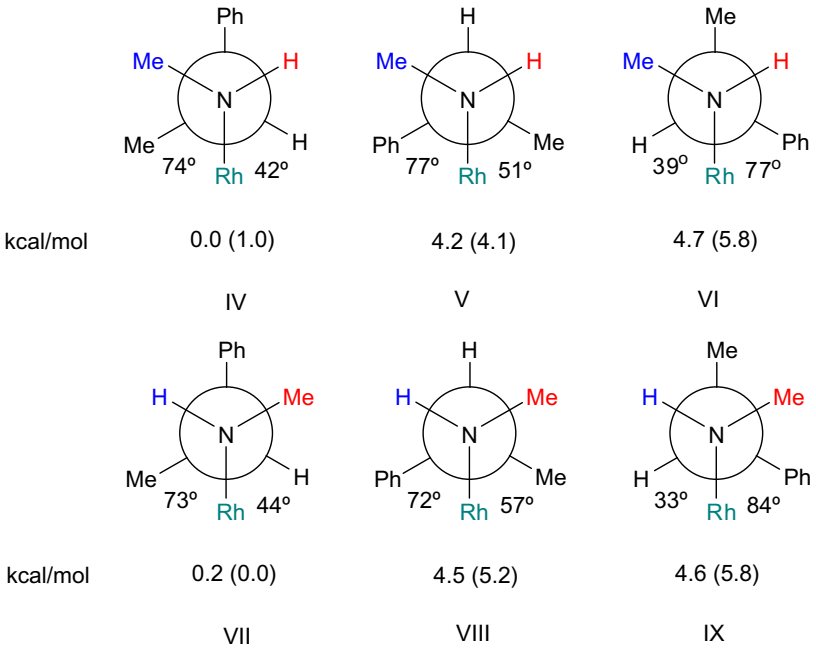

Figure 7. Six conformers (C_SN_R and C_SN_S) of the 1:1 Rh_2TFA_4-**2** adduct used as input for structure optimizations (for the sake of clarity, one Rh atom was shown), relative molecular energies and some structural parameters (dihedral angles Rh–N–C–CH_3, Rh–N–C–H, Rh–N–C–C^i). Energy calculations were performed for optimized structures applying either single molecule in vacuum or assuming the IEFPCM ($CHCl_3$) solvation model (in parentheses). Energies of the C_SN_R conformer **IV** (isolated molecule) or C_SN_S **VII** (solvated molecule) were assumed to be 0.0 kcal/mol.

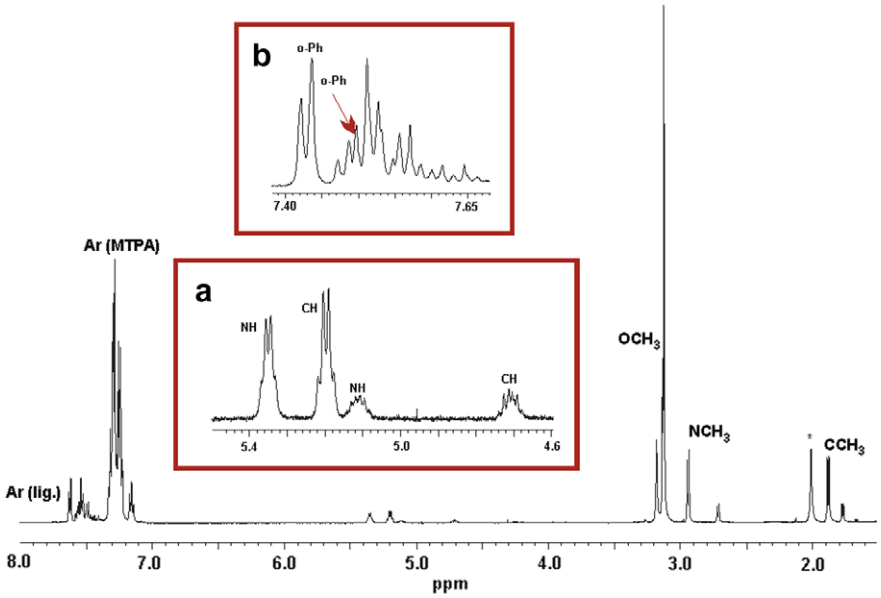

Figure 8. ^{1}H NMR spectrum of the 1:1 (4*S*)-Rh_2MTPA_4-**2** adduct ($CDCl_3$, 303 K). Insets show (a) the expansions of NH/CH and (b) Ph regions.

relationship, the large and small coupling constants were expected to correspond to anti-periplanar and gauche arrangements of the CH and NH bonds. The calculations performed for the two conformers of **2** (GIAO, B3LYP//6-311G++(2d,p)) provided the ^3J values of 8.8 and 1.1 Hz. In conclusion, structures **IV** and **VII** were tentatively identified as the major and minor adducts, respectively.

The NOE experiments provided independent and unambiguous evidence. For the major adduct the inversion of the CCH_3 signal caused the enhancement of the CH, Ph_{ortho} and NCH_3 signals; inversion of the CH signal enhanced the CCH_3, Ph_{ortho} and NH signals. These last three signals are perturbed also during NCH_3 inversion. Finally, inversion of the NH enhanced the CH, Ph_{ortho} and NCH_3 peaks. Such interaction patterns unambiguously identified the major adduct Rh_2MTPA_4-**2** as **IV**, with the C_SN_R configuration. For the minor component, the inversion of CCH_3 caused an increase of CH, Ph_{ortho} and NH signals, whereas inversion of the CH perturbed the intensities of CCH_3, Ph_{ortho} and NCH_3 peaks. The inversion of the NCH_3 signal resulted in one NOE interaction, with the NH signal; inversion of the CH resulted in two interactions with the CCH_3 and NCH_3. However, all lacking interactions were found in a NOESY 2D spectrum. These NOE interactions identified the minor component as **VII**, having the C_RN_S configuration.

2.3. Adducts of (*S*)-*N*-ethyl-1-phenylethylamine 3

Since the mixture of rhodium tetratrifluoroacetate and **3** decomposed rapidly, the Rh_2TFA_4-**3** adduct was not studied by advanced NMR techniques. Nevertheless, this adduct was used as a model molecule for computations. Two configurations at the nitrogen atom and all the arrangements around N–C and N–CH_2 bonds resulted in 18 structures of the adduct (two diastereoisomers, nine conformers of each). Structure optimizations and molecular energy calculations were performed for all of these structures (Fig. 9). The results led us to the conclusion that molecular energy depended mainly on the arrangement of the substituents around the N–CH bond. Anti-periplanar conformations with Ph and Rh groups opposite to each other exhibited the lowest energy (Fig. 9, structures **X**, **XI** and **XII**). The arrangement of the ethyl group (rotation around CH–CH_2 bond) provided the smallest contribution to the energy (cf. structures **X**, **XIII** and **XIV**). Finally, two diastereoisomers, C_SN_R **XIV** and C_SN_S **XV**, were expected to exist in the mixture of dirhodium salt and **3**.

Although the calculations were performed for Rh_2TFA_4-**3**, we assumed that the results applied also to Rh_2MTPA_4-**3**. In fact, the spectrum of Rh_2MTPA_4 and **3** (1:0.5 mixture) contained the signals of two adducts, with molar ratio of ca. 1:10. Each of the dirhodium salt [(4*S*) and (4*R*)] behaved similarly and formed the same mixture of adducts; there were no significant differences in ^1H and ^{13}C chemical shifts between the (4*R*)- and (4*S*)-diastereoisomers (Table 1). The signals of the minor components, due to low intensities and overlapping were difficult to detect, and only careful inspection of the 2D spectra (^1H,^1H COSY and ^{13}C,^1H gHSQC) allowed signal identifications and assignments. The same reasons made it difficult to estimate the diastereomerization rate in the mixture, and to apply NOE techniques to the minor adduct. In contrast, NOE experiments (truncated driven NOE, at 303 K) were successful in case of the main adduct. Apart from irrelevant NOE interactions between substituents attached to the same carbon atom (e.g., between CCH_3, Ph_{ortho} and CH groups, or between NH and Et), some diagnostic enhancements were noted. Namely, saturation of the NH signal resulted in answers of Ph_{ortho} and CH signals; saturation of the low-frequency signal of the CH_2 group (at 3.25 ppm) enhanced the signal of CCH_3 and Ph_{ortho} groups. It is noteworthy that there was no reaction of the Ph_{ortho} signal during irradiation of the high-frequency CH_2 peak (at 3.47 ppm); this suggests that only one hydrogen atom from CH_2 group was close to Ph. Hence, the rotation around CH–CH_2 bond was hindered and the particular arrangement of the ethyl group was fixed. Irradiation of CCH_3 resulted in the answer of both CH_2 signals; irradiation of the Ph enhanced

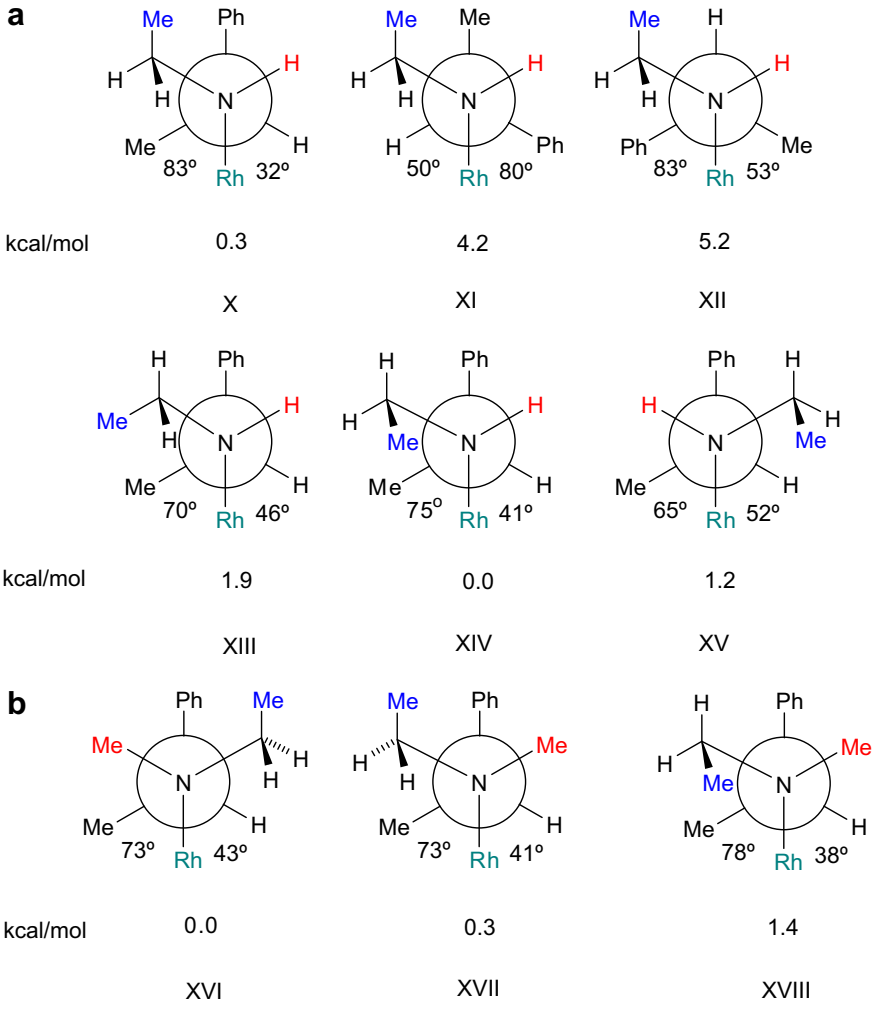

Figure 9. Selected conformers of (a) 1:1 Rh_2TFA_4-**3** (**X**–**XV**) and (b) Rh_2TFA_4-**4** (**XVI**–**XVIII**) used as input for structure optimizations, relative molecular energies and some structural parameters (dihedral angles Rh–N–C–CH_3, Rh–N–C–CH_2, Rh–N–C–H, Rh–N–C–C^i). Energies of **XIV** (Rh_2TFA_4-**3** set) and **XVI** (Rh_2TFA_4-**4** set) were adjusted to 0 kcal/mol. For the sake of clarity, one Rh atom is shown. All calculations were performed for single molecule in vacuum. The figure represents the structures exhibiting the lowest molecular energy.

the NH peak. However, saturation of the CH peak provided only non-diagnostic interactions, with Ph_{ortho} and CCH_3 protons. The above NOE interactions, although incomplete, unambiguously identified the main isomer of Rh_2MTPA_4-**3** as C_SN_R (**X** or **XIV**).

Despite the lack of NOE data, two arguments suggested C_SN_S configuration of the minor adduct, there were a COSY experiment and ^{13}C NMR data. The minor adduct produced a cross peak between the CH and NH hydrogens in the COSY spectrum; lack of the corresponding cross peak in the case of the main adduct. This finding indicated a larger ^3J(CH,NH) value in the minor adduct and are smaller in the main one. By analogy to Rh_2TFA_4-**2**, one can conclude that the minor and major adducts contain anti-periplanar and gauche arrangements of CH and NH bonds, respectively (structures **XV** and **XIV**). On the other side, differences in ^{13}C chemical shifts between C_SN_R and C_SN_S diastereoisomers exhibited similar features for all pairs of **2** and **3** adducts. The signals of CCH_3 and NCH_3 (or NCH_2) groups were especially diagnostic. For instance, the pair of (4*S*)-Rh_2MTPA_4-**2** diastereoisomers exhibited negative $\delta(C_SN_R)-\delta(C_SN_S)$ values of −10.0 ppm for CCH_3 and −8.0 ppm for the NCH_3 methyl groups. Analogous differences between major and minor (4*S*)-Rh_2MTPA_4-**3** adducts were −9.3 ppm (CCH_3) and −5.0 ppm (NCH_2). Finally, the best linear correlation between the calculated and experimental ^{13}C data was found assuming a C_SN_R configuration for the main adduct and a C_SN_S configuration for the secondary adduct.

2.4. Adducts of (*S*)-*N*-ethyl-*N*-methyl-1-phenylethylamine 4

Each of the investigated dirhodium salts Rh_2TFA_4 and Rh_4MTPA_4 [(4*S*) and (4*R*)] formed two adducts in the solution in the molar ratio of 1:1.5 (Rh_2TFA_4-**4**) and 1:1.8 (Rh_2MTPA_4-**4**). The diastereomerization rate was evaluated by selective inversion recovery experiments and came to ca. 1 s^{-1} for Rh_2TFA_4-**4** (at 270 K) and less than 1 s^{-1} for Rh_2MTPA_4-**4** (263 K). However, the rate of Rh_2TFA_4-**4** increased up to ca. 10 s^{-1} at 303 K. Structure optimization and molecular energy calculations performed for all 18 conformers/diastereoisomers allowed us to select the structures **XVI** and **XVII** as the most likely adducts in the mixture (Fig. 9). Both diastereoisomers were expected to appear in ca. 1:1 molar ratio (energy difference of 0.3 kcal/mol).

Unfortunately, NOE experiments failed in the case of these adducts. Only unimportant NOE interactions were detected for Rh_2TFA_4-**4** (303 K), namely, some interactions between CCH_3 and Ph_{ortho} or CH hydrogen atoms. Negative results may be caused either by the fast ligand exchange or/and by fast rotation around the N–C bond. Some signal overlapping was another impediment to the measurements. On the other hand, a temperature decrease resulted in signal broadening. In the case of Rh_4MTPA_4-**4**, difficulties arose from signal proximity and overlapping. Although inspection of 2D spectra allowed the identifications of all ^1H and ^{13}C signals, the application of any selective experiment was impossible.

Carbon chemical shifts were the only mean of structure identification. The conformer **XVI** with a C_SN_S configuration was an analogue of (C_SN_R)-Rh_2MTPA_4-**2** as far as the methyl group was considered, or of (C_SN_S)-Rh_2MTPA_4-**3** with regard to the CH_2 group. Diastereomeric dispersion was calculated as a chemical shift difference between N_R and N_S adducts which was negative for both the NCH_3 group in Rh_2MTPA_4-**2** (−8 ppm) and the CH_2 group in Rh_2MTPA_4-**3** (−5 ppm). Thus, the chemical shift difference between **XVI** (C_SN_S) and **XVII** (C_SN_R) was expected to be the same (i.e., negative) similar to Rh_2MTPA_4-**2** for the NCH_3 group and opposite (positive) than in Rh_2MTPA_4-**3** for the CH_2 group. These conditions were satisfied if the major Rh_2MTPA_4-**4** adduct was assigned to **XVI** and minor one to **XVII** (Table 1). The same applied to Rh_2TFA_4-**4** adducts. Correlations of theoretically calculated and experimental ^{13}C chemical shifts provided additional evidence. The correlation was better assuming the assignment shown in Table 1 than in the opposite case.

2.5. The application of experimental and calculated ^{13}C NMR chemical shifts

The carbon chemical shifts of adducts studied in the present work exhibited interesting features which appeared to be very helpful for structure determination. These subjects are worthy of re-capitulation. To begin with, in order to verify the configuration assignments, the computation of ^{13}C chemical shifts and the linear regression between theoretical and experimental data were performed (Tables 1 and 5). Only the signals of CH, CH_3, NCH_3 and NCH_2CH_3 groups were considered; the signals of Ph groups were omitted as troublesome for identification and not diagnostic. For the sake of simplification, the calculations were performed for Rh_2TFA_4 adducts only; these theoretical data were correlated with the chemical shifts of both Rh_2TFA_4 and Rh_2MTPA_4 adducts. The regressions were checked for each pair of diastereoisomers, that is, experimental data for C_SN_R and C_SN_S diastereoisomers together as one set were correlated with the corresponding theoretical values assuming configuration assignment either like that in Table 1 or opposite. Despite such simplifications, the results were unambiguous. Standard errors associated with linear regression (rms), measuring how closely data points spread about regression, line appeared to be especially significant. Depending on the rhodium salt (Rh_2TFA_4 or Rh_2MTPA_4), the best correlations (rms from 0.6 to 2.1; *R* from 0.997 to 1.000) were found if the configurations at the nitrogen atom, such as those in the Table 1 were assumed. Opposite assignments provided poor results (rms from 5.9 to 10.7, *R* 0.909 to 0.974). Hence, theoretical findings supported the experimental conclusions (however, one should bear in mind that some structures were identified by ^{13}C chemical shift only, e.g., adducts of **4**).

Two parameters related to NMR were commonly used for describing the complexation: complex (or adduct) formation shift $\Delta\delta$ (ppm) defined as chemical shift difference of a signal in the adduct and free ligand, and diastereomeric dispersion $\Delta\nu$ (Hz) specified as chemical shift difference of a signal in the two diastereoisomers.[19] These two parameters concerning the ^{13}C data of dirhodium adducts are shown in Table 6. Assuming the same convention for all adducts, $\Delta\delta = \delta_{complex} - \delta_{free\ ligand}$ and $\Delta\nu = \delta(C_SN_R) - \delta(C_SN_S)$, one could attribute a sign to each of $\Delta\delta$ and $\Delta\nu$. For the sake of comparison, $\Delta\nu$ was expressed in ppm.

Rh_2TFA_4-**1** contains two *N*-methyl groups, one pro-*R* (38.8 ppm), anti-periplanar to the CH hydrogen, and pro-*S* (48.5 ppm), gauche to CH. The corresponding $\Delta\delta$ values are negative and positive, of −4.3 and 5.4 ppm. The chemical shift difference $\delta_{pro\text{-}R}-\delta_{pro\text{-}S}$, which can be regarded as dispersion, is negative (−9.7 ppm). All adducts of **2** and **3**, with C_SN_R configurations and NCH_3 (NCH_2) groups anti-periplanar to CH hydrogen, exhibit negative $\Delta\delta$ for these groups, from −1.9 to −4.7 ppm, whereas C_SN_s adducts display positive $\Delta\delta$, from 2.9 to 3.5 ppm. The diastereoisomeric dispersion of NCH_3 (NCH_2) is negative and varied from −4.8 to −8.0 ppm. CCH_3 groups exhibit large negative $\Delta\nu$, of ca. −10 ppm, although $\Delta\delta$ values for both diastereoisomers are negative. One can also find some trends in $\Delta\delta$ and $\Delta\nu$ for CH carbon atom (Table 6).

The adducts of **4** require some comment. Due to the two alkyl groups at the nitrogen atom, CH_3 and CH_2CH_3, C_SN_R adducts of **4** correspond to the C_SN_S adducts of **2** with regard to the *N*-methyl group, but to C_SN_R adducts of **3** if one considers *N*-ethyl group. Consequently, the adducts of **4** exhibit positive $\Delta\nu$ for NCH_3, and negative $\Delta\nu$ for NCH_2, that is, with the opposite and the same sign than the remaining adducts, respectively. The $\Delta\delta$ of CH and CCH_3 groups is not diagnostic in the case of **4**.

Table 5
Calculated ^{13}C chemical shifts (ppm) and diastereomeric dispersions $\Delta\nu$ (in parentheses, ppm) for the adducts of Rh_2TFA_4 with amines **1–4**[a]

Adduct			CH	CCH_3	Ph(C^i)	NCH_3	NCH_2CH_3	NCH_2CH_3
Rh_2TFA_4-**1**	**I**		75.9	20.7	146.1	41.1[b], 50.7[c](−9.6)[d]		
			72.4	20.7	147.9	39.6[b], 47.5[c]		
Rh_2TFA_4-**2**	**IV**	N_R	66.6(−4.2)	13.8(−11.3)	147.5(−1.7)	30.5(−8.9)		
			65.2	14.8	150.3	29.6		
	VIII	N_S	70.8	25.1	149.2	39.4		
			68.8	24.6	152.8	37.1		
Rh_2TFA_4-**3**	**XIV**	N_R	67.1(−4.3)	14.2(−11.8)	148.0(−2.9)	—	45.7(−4.8)	16.4(0.2)
			64.5	15.1	151.5	—	42.2	16.0
	XV	N_S	71.4	26.0	150.9	—	50.5	16.2
			68.3	24.6	155.6	—	47.4	16.1
Rh_2TFA_4-**4**	**XVII**	N_R	74.5(−0.7)	19.1(−2.1)	146.8(−1.9)	45.0(8.0)	54.9(−6.3)	13.0(0.5)
			70.8	19.2	149.5	42.3	52.8	10.5
	XVI	N_S	75.2	21.2	148.7	37.0	61.2	12.5
			71.7	21.0	152.3	34.8	56.1	9.7

[a] Dispersions $\Delta\nu$ were calculated as difference $\delta(C_SN_R) - \delta(C_SN_S)$. The first entry for each structure contains chemical shifts and $\Delta\nu$ of an adduct; the second entry concerns chemical shifts calculated for ligand fragment while dirhodium unit is removed (see explanation in the text). All calculations were performed for a single molecule in vacuum.
[b] Pro-*R* *N*-methyl signal.
[c] Pro-*S* *N*-methyl signal.
[d] The dispersion (ppm) was calculated as $\delta_{\text{pro-}R} - \delta_{\text{pro-}S}$.

Table 6
^{13}C adduct formation shift $\Delta\delta$ and diastereomeric dispersions $\Delta\nu$ (in parenthesis) for some adducts of dirhodium salts with amines **1–4**[a]

Adduct		T (K)	CH	CCH_3	NCH_3	NCH_2CH_3	NCH_2CH_3
Rh_2TFA_4-**1**		303	1.1	−2.2	−4.3[b], 5.4[c](−9.7)[d]		
Rh_2TFA_4-**2**	N_R	263	−0.7(−4.3)	−9.6(−8.1)	−3.8(−7.3)		
	N_S		3.6	−1.5	3.5		
(*4S*)-Rh_2MTPA_4-**2**	N_R	303	−1.4(−4.9)	−10.6(−10.0)	−4.7(−8.0)		
	N_S		3.5	−0.6	3.3		
(*4S*)-Rh_2MTPA_4-**3**	N_R	273	0.0(−3.4)	−10.2(−9.3)	—	−2.0(−5.0)	−0.1(0.9)
	N_S		3.4	−0.9	—	3.0	−1.0
(*4R*)-Rh_2MTPA_4-**3**	N_R	273	0.3(−3.2)	−10.1(−9.0)	—	−1.9(−4.8)	−0.1(0.7)
	N_S		3.5	−1.1	—	2.9	−0.8
Rh_2TFA_4-**4**	N_R	273	6.2(1.0)	−0.4(0.2)	5.9(8.3)	−0.4(−7.9)	−2.1(−0.5)
	N_S		5.2	−0.6	−2.4	7.5	−1.6
(*4S*)-Rh_2MTPA_4-**4**	N_R	303	6.0(0.6)	0.4(0.0)	6.1(8.7)	−0.1(−7.6)	−1.4(−0.3)
	N_S		5.4	0.4	−2.6	7.5	−1.1
(*4R*)-Rh_2MTPA_4-**4**	N_R	303	6.1(1.0)	0.2(−0.2)	5.9(8.4)	−0.1(−7.2)	−1.7(−0.2)
	N_S		5.1	0.4	−2.5	7.1	−1.5

[a] The $\Delta\delta(^{13}C)$ and $\Delta\nu(^{13}C)$ values (ppm) were calculated for 1:1 adducts on the basis of Table 1, according to formulas $\Delta\delta = \delta_{\text{adduct}} - \delta_{\text{free ligand}}$ and $\Delta\nu = \delta(C_SN_R) - \delta(C_SN_S)$. The values arising from the main isomers are underlined.
[b] Pro-*R* *N*-methyl signal.
[c] Pro-*S* *N*-methyl signal.
[d] The dispersion (ppm) was calculated as $\delta_{\text{pro-}R} - \delta_{\text{pro-}S}$.

As was aforementioned, the calculated chemical shifts correlated well with the experimental data and can be used for structure identification. It is difficult to calculate the $\Delta\delta$ parameter reasonably because calculated chemical shifts of an adduct concern a particular conformation, whereas reference data of free ligand consist of averaged chemical shifts originating from a few conformers with unknown populations. However, one can calculate easily $\Delta\nu$; these values (Table 6) reproduce well experimental findings.

The last question concerns the origin of $\Delta\delta$ and $\Delta\nu$, that is, whether they are caused by the dirhodium unit or by particular arrangements of the substituents in a ligand. In order to explore this subject, we performed chemical shift calculations for the molecules obtained from optimized adduct structure by simple deletion of the dirhodium unit. The structures of such molecules were far from optimum, but exhibited the same structural features like those in adducts. Chemical shifts obtained by this way differed slightly from those in adducts, but were qualitatively similar. Concluding, mainly the arrangement of substituents in the ligand fragment determined the magnitude of $\Delta\delta$ and $\Delta\nu$.

3. Conclusion

Each of the enantiomerically pure amines **2–4** forms with rhodium(II) salts in $CDCl_3$ solutions two diastereoisomeric adducts, with C_SN_R and C_SN_S configurations. The lifetimes of the diastereoisomers are relatively long (in NMR time scale); the signals of all species can be observed conveniently at room temperature (303 K) or moderately decreased temperature (263–273 K). Diastereomerization rates, depending on the temperature, vary from ca. 10 to much less than 1 s^{-1}. Apart from slow diastereomerization, the adducts exist as relatively stable conformers.

Configurations at the nitrogen atom were determined with respect to a carbon centre by NOE experiment, at least in most cases. NOE build-up measurements provided qualitatively interatomic distances in molecules. The alternative NULL method failed, probably due to short relaxation time T_1 of protons in adducts.

Carbon-13 data (chemical shift δ, adduct formation shift $\Delta\delta$ and diastereomeric dispersion $\Delta\nu$) exhibit some features which can be very useful in studies on configuration. Computed optimal adduct structures and calculated chemical shifts were in agreement with

the experimental results and provided supporting structural information.

4. Experimental

4.1. Syntheses

All amines were obtained from commercially available primary (*S*)-1-phenylethylamine according to the described procedures. Tertiary (*S*)-*N*,*N*-dimethyl-1-phenylethylamine **1** was obtained from the primary amine by the methylation with formic acid and formic aldehyde.[28] Secondary (*S*)-*N*-methyl-1-phenylethylamine **2** was obtained by the reaction with methyl chloroformate and subsequent reduction with $LiAlH_4$.[29] (*S*)-*N*-Ethyl-1-phenylethylamine **3** was prepared by the acetylation of primary amine and subsequent reduction with $LiAlH_4$. (*S*)-*N*-Ethyl-*N*-methyl-1-phenylethylamine **4** was obtained from **3** by the reaction with formic acid and formic aldehyde.[28] Rhodium(II) tetra-α-methoxy-α-(trifluoromethyl)-phenylacetate dimer (4*R*) and (4*S*) were prepared from commercially available dirhodium tetraacetate and enantiomerically pure Mosher's acid (MTPA).[30] Rhodium(II) tetraacetate and rhodium(II) tetratrifluoroacetate were commercially available and were purchased from Aldrich.

4.2. Structure optimization and shielding calculations (DFT)

GAUSSVIEW 3.0 and GAUSSIAN 03 package[31] have been used for the construction of molecules and all DFT calculations. Structure optimizations of adducts were performed at 3-21G//B3LYP theory level. Electronic energies and NMR shieldings (GIAO) were calculated by the B3LYP method using LANL2DZ basis set for rhodium atoms and 6-311G(2d,p) basis set for H, C, N, O and F atoms. Calculations were performed either assuming the single molecule in vacuum or applying IEFPCM solvation model ($CHCl_3$). Shielding scales were recalculated to chemical shift scales using reference shielding incorporated in GAUSSIAN package, of 31.88 ppm for ^1H (0 ppm, TMS) and 182.47 ppm for ^{13}C (0 ppm, TMS). $^3J(^1H,^1H)$ coupling constants were calculated using B3LYP//6-311G++(2d,p) theory level.

4.3. NMR measurements

All NMR experiments were run on a BRUKER DRX-500 Avance spectrometer with XWINNMR acquisition and processing software, equipped with a 5-mm triple broadband inverse probe (TBI) with z-gradient coil. The sample temperatures (from 268 to 318 K) were adjusted using the instrument temperature panel, and temperature readings were taken without further corrections. Standard parameter sets were applied for conventional ^1H and ^{13}C NMR spectra. All measurements were taken in $CDCl_3$ (99.8% D atom stabilized by Ag); solvent signals were used as secondary references: 7.26 ppm (^1H) and 77.0 ppm (^{13}C). A typical sample contained ca. 10 mg of dirhodium salt and 0.5 equiv of a ligand; such a ratio ensured the presence of one adduct (1:1) in the mixture. All samples for NOE, EXSY and T_1 measurements were deoxygenated by four freeze–pump–thaw cycles, using J. Young valve NMR-tubes.

The measurements of relaxation times T_1 were carried out by standard inversion recovery sequence D1–180°–VD–90°–AQ (Bruker's 'irt1' pulse programme). The NULL experiment (inversion recovery measurements with all but one signal inverted)[27] was achieved by D1–180°_{sel}–180°–VD–90°–AQ pulse sequence. The chemical exchange was studied by the use of D1–180°_{sel}–VD–90°–AQ sequence. Typical parameters for all the above experiments were as follows: a relaxation delay D1 from 6 to 10 s, an acquisition time AQ of 2.7 s, sweep width of 12 ppm, a data matrix of 32 K (32 K) and number of scans either 8 or 16 per FID. Typical VD list included 0.01, 0.05, 0.1, 0.18, 0.25, 0.5, 0.75, 1.0, 1.5, 2.0, 3.5, 5.0 and 10.0 s delays. Selective 180° pulse (i-SNOB[32]) from 10 to 80 ms depending on the desired selectivity was applied for the selective inversion. NOE measurements were performed using DPFGSE-NOE 1D technique (Bruker's 'selnogp.3' pulse programme) with the parameters: a relaxation delay of 3 s, number of scans either 64 or 128 and mixing times from 30 to 250 ms. The remaining parameters were as mentioned above. EXSY 2D spectra were acquired using a NOESY 2D sequence (Bruker's 'noesyst' programme, phase sensitive using States-TPPI method), with the parameters: a relaxation delay of 1.2 s, sweep width of 8 ppm, an acquisition time of 0.26 s, number of scans of 8 and a $2048 \times 256(2048 \times 2048)$ data matrix. Mixing times from 100 to 300 ms were applied.

NOE build-up measurements were achieved by means of DPFGSE-NOE, using five to six mixing times from 25 to 220 ms. NOE enhancements were referred to intensity of inverted signal at 0 ms mixing time (Bruker's 'lastcal' command), assuming signal intensities of 100, 200 and 300 for CH, Ph_{orto} and CH_3 groups, respectively. NOE enhancements were plotted against mixing time; in case of deviation from linearity the points corresponding to long mixing times were removed. Then NOE build-up rates were extracted from the plot as a line slope. Atomic distances d(H–H) were read out from optimized structures **I**–**III**. Distances between CH_3, CH and Ph_{ortho} groups were obtained by averaging of all individual H–H atomic distances d according to the formula $(\langle d^{-3}\rangle^{-1/3}) = (\sum d_i^{-3})/i)^{-1/3}$ (i.e., three d(H–H) values were averaged in order to obtain d(CH–CH_3), six values for d(Ph_{ortho}–CH_3), etc).[26] Experimental distances d_x were estimated by the formula $d_x = d_{ref}(\sigma_{ref}/\sigma_x)^{1/6}$, using a theoretical distance as a reference and NOE build-up coefficients from Table 4 as σ. For simplification, the calculations were performed for each kind of interaction separately; for instance when the Ph_{ortho} signal was inverted, d(CCH_3–Ph_{ortho}) = 3.26 Å and NOE build-up rate of CCH_3 group (9.4) were used as reference values. Then NOE build-up rates of both NCH_3 groups (4.8 and 7.3) were used for the calculation of two NCH_3–Ph_{ortho} distances (3.65 and 3.4 Å). The calculations were repeated using build-up rates on Ph_{ortho} signal, obtaining distances of 3.62 and 3.29 Å. Averaging provided the values of 3.63 and 3.34 Å (Table 4).

4.4. Data treatment and estimation of exchange rates

All data treatments were performed using the Mathcad 2001 Professional programme. Standard procedures were applied for linear regressions and curves fitting (Matcad's 'line' and 'MinErr' procedures). The quality of a least squares fitting was expressed as the Pearson correlation coefficient R and standard error rms (Matcad's 'corr' and 'stderr' procedures).[33]

Exchange and diastereomerization rates were estimated using the general equation describing the evolution of perturbed two-site, equally populated systems under slow-exchange conditions:[23]

$$M_1(t) = M_1(\infty) - 0.5(e^{-(r+2k)t} + e^{-rt})[M_1(\infty) - M_1(0)] - 0.5(-e^{-(r+2k)t} + e^{-rt})[M_2(\infty) - M_2(0)]$$

where $M_1(t)$ denotes the magnetization of site 1 as a function of time t; $M_1(\infty)$ and $M_2(\infty)$ represent the equilibrium magnetization of sites 1 and 2, respectively; $M_1(0)$ and $M_2(0)$ represent the magnetization at time 0 (i.e., at the beginning of the experiment, immediately after selective 180° pulse); k is the exchange rate from site 1 to 2 and r denotes the relaxation rate $1/T_1$. If both sites were perturbed equally (bi-selective inversion), the equation was converted to

$$M(t)/M(\infty) = 1 - (1 + a)e^{-rt} \quad (1)$$

where coefficient a denotes a non-ideal inversion ($0 < a < 1$). If one signal was inverted, the evolutions of inverted and non-perturbed signals were described by Eqs. (2) and (3), respectively:

$$M_1(t)/M_1(\infty) = 1 - 0.5(1+a)(e^{-(r+2k)t} + e^{-rt}) \quad (2)$$

$$M_1(t)/M_1(\infty) = 1 - 0.5(1+a)(-e^{-(r+2k)t} + e^{-rt}) \quad (3)$$

The measurement and exchange rate estimation were performed for 1:0.5, 1:2 and 1:4 mixtures of Rh_2TFA_4 and **1**, that is, for the solutions containing the 1:1 adduct, 1:2 adduct or equimolar amounts of the 1:2 adduct and free amine, respectively.Evolutions of magnetization $M(t)$ as a function of time were obtained from selective inversion recovery experiment. Either NCH_3 signals (first two samples) or CCH_3 signals (1:4 sample) were used. Typically, both signals of each sample were inverted, one by one; giving totally four data sets for each sample at given temperature. The initial value of a, essential for MinErr algorithm, was estimated on the basis of $M(t)$ and $M(\infty)$, taken from the first experiment (VD delay of 10 ms); guess k value was assumed to be 1 s^{-1}. The parameters a and k were obtained by curve fitting procedure, using Eq. (2) for inverted signal and (3) for non-inverted signal. In the theory, one can perform a fitting procedure using three parameters, k, a and r simultaneously. However, the attempt to do it often resulted in non-realistic values, without physical meaning (for instant $k < 0$ or a drastically differs than expectation). Finally, the best results were obtained when r was assumed as a known parameter, taken from bi-selective inversion recovery experiment using the Eq. (1). Such simplification did not significantly influence the results.Since both NCH_3 groups are located at the same nitrogen atom, the NOE enhancement of non-perturbed NCH_3 signal was expected during selective inversion experiment.[26] Such effect was noted in some measurements (Fig. 3). However, the inclusion of the NOE in Eq. (2) did not improve significantly the data fitting.For two-site system with unequal populations the following equation was used

$$M_1(t) = M_1(\infty) - A[M_1(\infty) - M_1(0)] - B[M_2(\infty) - M_2(0)]$$

where $A = [kfe^{-(r+kf+kr)t} + kre^{-rt}]/[kf + kr]$, $B = [kr(-e^{-(r+kf+kr)t} + e^{-rt})]/[kf + kr]$, kf and kr state forward and reverse exchange rates, respectively. By analogy to Eqs. (2) and (3), this equation converted to (4) and (5) for selectively inverted and non-perturbed signals, respectively:

$$M_1(t)/M_1(\infty) = 1 - A(1+a) \quad (4)$$

$$M_1(t)/M_1(\infty) = 1 - B(1+a)M_2(\infty)/M_1(\infty) \quad (5)$$

The equations contain four parameters to fit, r, kf, kr and a. However, an attempt to fit all parameters simultaneously resulted in a large spread of kf and kr values, depending on the signal used for the calculations. The best results were obtained assuming a and r as known parameters (estimated from signal integrals and bi-selective T_1 measurement) and fitting only kf and kr.The exchange rate k ($k_1 + k_{-1}$) estimations from 2D EXSY spectra were achieved using the equation $\exp(-t_m/2k) = (1-b)/(1+b)$, where t_m denotes mixing time and b states the ratio of the cross peak to diagonal peak volume.[24]

References

1. Cotton, F. A.; Walton, R. A. *Multiple Bonds Between Metal Atoms*; Claredon Press: Oxford, 1993. Chapter 7, pp 431.
2. Clayden, J.; Greeves, N.; Warren, S.; Wothers, P. *Organic Chemistry*; Oxford University Press: Oxford, 2001. p. 1057.
3. Doyle, M. *J. Org. Chem.* **2006**, *71*, 9253–9260.
4. Hansen, J.; Davies, H. *Coord. Chem. Rev.* **2008**, *254*, 545–555. and references cited therein.
5. Katsaros, N.; Anagnostopoulou, A. *Crit. Rev. Oncol. Hematol.* **2002**, *42*, 297–308.
6. Deubel, D. *J. Am. Chem. Soc.* **2008**, *130*, 665–675.
7. Burda, J.; Gu, J. *J. Inorg. Biochem.* **2008**, *102*, 53–62.
8. Kang, M.; Chitofides, H.; Dunbar, K. *Biochemistry* **2008**, *47*, 2265–2276.
9. Chitofides, H.; Dunbar, K. *J. Am. Chem. Soc.* **2007**, *129*, 12480–12490.
10. Aguirre, J.; Lutterman, D.; Angeles-Boza, A.; Dunbar, K.; Turro, C. *Inorg. Chem.* **2007**, *46*, 7494–7502. and references cited therein.
11. Frelek, J.; Górecki, M.; Jaźwiński, J.; Masnyk, M.; Ruśkowska, P.; Szmigielski, R. *Tetrahedron: Asymmetry* **2005**, *16*, 3188–3197.
12. Frelek, J.; Jaźwiński, J.; Masnyk, M.; Ruśkowska, P.; Szmigielski, R. *Tetrahedron: Asymmetry* **2005**, *16*, 2437–2448.
13. Frelek, J.; Klimek, A.; Ruśkowska, P. *Curr. Org. Chem.* **2003**, *7*, 1081–1104.
14. Frelek, J.; Jagodziński, J.; Meyer-Figge, H.; Sheldrick, S.; Wieteska, E.; Szczepek, J. *Chirality* **2001**, *13*, 313–321.
15. Frelek, J. *Tetrahedron: Asymmetry* **1999**, *10*, 2809–2816.
16. Frelek, J.; Szczepek, J. *Tetrahedron: Asymmetry* **1999**, *10*, 1507–1520.
17. Frelek, J. *Pol. J. Chem.* **1999**, *73*, 229–239.
18. Frelek, J.; Geiger, M.; Voelter, W. *Curr. Org. Chem.* **1999**, *3*, 117–146.
19. Duddeck, H. *Chem. Rec.* **2005**, *5*, 396–409. and references cited therein.
20. Jaźwiński, J. *J. Mol. Struct.* **2005**, *750*, 7–17.
21. Jaźwiński, J. *Tetrahedron: Asymmetry* **2006**, *17*, 2358–2365.
22. Jaźwiński, J.; Kamieński, B. *Solid State NMR* **2007**, *32*, 25–33.
23. Bain, A.; Cramer, J. *J. Phys. Chem.* **1993**, *97*, 2884–2887.
24. Bain, A. *Prog. Nucl. Magn. Reson. Spectrosc.* **2003**, *43*, 63–103.
25. Chesnut, D. *Chem. Phys. Lett.* **2003**, *380*, 251–257.
26. Neuhaus, D.; Williamson, M. *The Nuclear Overhauser Effect in Structural and Conformational Analysis*; VCH: New York, 1989.
27. Liu, M.; Farrant, D.; Lindon, J. *Magn. Reson. Chem.* **1992**, *30*, 173–176.
28. Icke, R.; Wisegarver, B.; Alles, G.. In *Org. Synth.*; John Wiley and Sons: New York, 1955; Coll. Vol. III.
29. Pallavicini, M.; Valloti, E.; Villa, L.; Resta, I. *Tetrahedron: Asymmetry* **1994**, *5*, 363–370.
30. Wypchlo, K.; Duddeck, H. *Tetrahedron: Asymmetry* **1994**, *5*, 27–30.
31. Frisch, M. J.; Trucks, G. W.; Schlegel, H. B.; Scuseria, G. E.; Robb, M. A.; Cheeseman, J. R.; Montgomery, J. A., Jr.; Vreven, T.; Kudin, K. N.; Burant, J. C.; Millam, J. M.; Iyengar, S. S.; Tomasi, J.; Barone, V.; Mennucci, B.; Cossi, M.; Scalmani, G.; Rega, N.; Petersson, G. A.; Nakatsuji, H.; Hada, M.; Ehara, M.; Toyota, K.; Fukuda, R.; Hasegawa, J.; Ishida, M.; Nakajima, T.; Honda, Y.; Kitao, O.; Nakai, H.; Klene, M.; Li, X.; Knox, J. E.; Hratchian, H. P.; Cross, J. B.; Adamo, C.; Jaramillo, J.; Gomperts, R.; Stratmann, R. E.; Yazyev, O.; Austin, A. J.; Cammi, R.; Pomelli, C.; Ochterski, J. W.; Ayala, P. Y.; Morokuma, K.; Voth, G. A.; Salvador, P.; Dannenberg, J. J.; Zakrzewski, V. G.; Dapprich, S.; Daniels, A. D.; Strain, M. C.; Farkas, O.; Malick, D. K.; Rabuck, A. D.; Raghavachari, K.; Foresman, J. B.; Ortiz, J. V.; Cui, Q.; Baboul, A. G.; Clifford, S.; Cioslowski, J.; Stefanov, B. B.; Liu, G.; Liashenko, A.; Piskorz, P.; Komaromi, I.; Martin, R. L.; Fox, D. J.; Keith, T.; Al-Laham, M. A.; Peng, C. Y.; Nanayakkara, A.; Challacombe, M.;Gill, P. M. W.; Johnson, B.; Chen, W.; Wong, M. W.; Gonzalez, C. J. A. *GAUSSIAN 03, Revision B.5*, Pople Gaussian: Pittsburgh PA, 2003.
32. Kupče, E.; Boyd, J.; Campbell, I. *J. Magn. Reson., Ser. B* **1995**, *106*, 300–303.
33. *Mathcad User's Guide with Reference Manual*, MathSoft, Cambridge, 2000, http://www.mathsoft.com/.